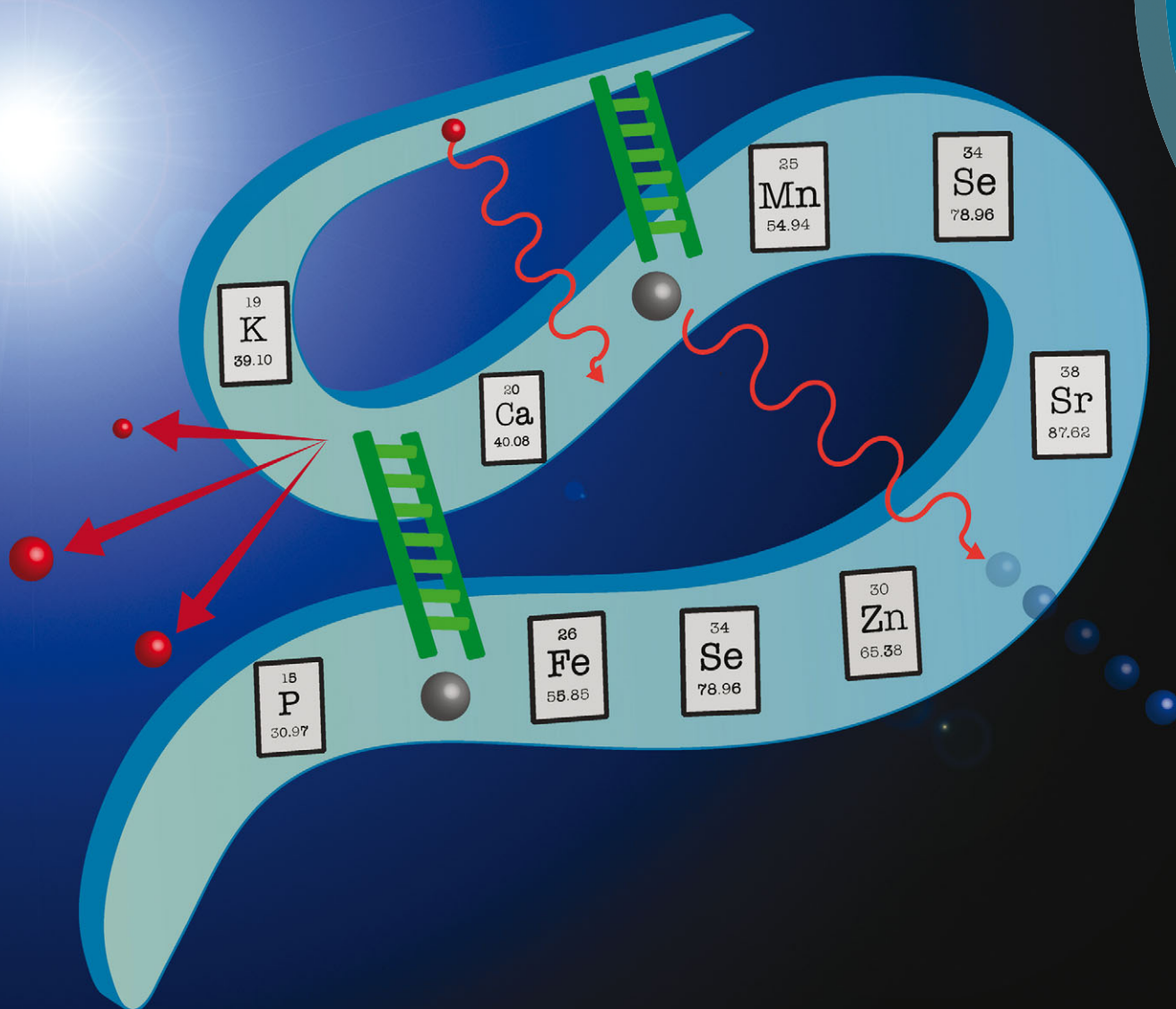


Metallomics

www.rsc.org/metallomics



ISSN 1756-5901



COMMUNICATION

Gawain McColl *et al.*

High-resolution complementary chemical imaging of bio-elements in *Caenorhabditis elegans*

Indexed in
Medline!



Cite this: *Metallomics*, 2016, 8, 156

Received 6th November 2015,
Accepted 9th November 2015

DOI: 10.1039/c5mt00288e

www.rsc.org/metallomics

High-resolution complementary chemical imaging of bio-elements in *Caenorhabditis elegans*[†]

Dominic J. Hare,^{‡ab} Michael W. M. Jones,^{‡cd} Verena C. Wimmer,^b
Nicole L. Jenkins,^b Martin D. de Jonge,^c Ashley I. Bush^b and Gawain McColl^{*b}

Here, we present a sub- μm multimodal approach to image essential elements in *Caenorhabditis elegans*. A combination of chemical imaging technologies reveals total metal concentration, chemical state and the protein to which an element is associated. This application of distinct yet complementary chemical imaging techniques provided unique insight into essential and trace elements at the subcellular level.

Caenorhabditis elegans is a model system that displays highly compartmentalised elemental distribution ranging from high abundance species to ultra-trace elements. When imaging these elements, abundance within the sample does not necessarily equate to high sensitivity or the capacity for high spatial resolution.¹ Application of synchrotron-based X-ray fluorescence microscopy (XFM) is no exception; a number of factors determine whether an analyte can be detected and spatially mapped at subcellular resolution. These factors relate to both technical limitations and the nature of the sample itself. Considerations for imaging elements in *C. elegans* include: the energy of the incident beam, duration of exposure, the atomic mass of the element, the energy of the fluorescence, the characteristics of the detector used, the composition and thickness of the sample, and the environmental conditions in which the analysis takes place.²

Fluorescence profiles of specific elements must be discerned from elastic (Rayleigh) and inelastic (Compton) scattering;³ *i.e.* element-specific fluorescence must not be obscured by scatter peak tails. The incident X-ray energy determines which excitation events can occur, but also positions the scattering

peaks within the X-ray spectrum. Lower mass (*Z*) elements have reduced cross-sections, fluorescent yields and are easily absorbed by the sample matrix, all limiting sensitivity. While self-absorption may be negligible for heavier elements in thinner specimens, it places real limitations on low-*Z* elements, even within single cells.^{4,5} In addition, for specimens measured in air, argon (Ar) fluorescence causes a major interfering peak in the collected spectra (with associated tail) that can overwhelm the signal derived from lighter bio-elements, making their detection impossible.⁶ Previously, within whole animals biologically important mid-*Z* elements, such as calcium (Ca), zinc (Zn) and redox-active metals have often been analysed without corresponding data on low-*Z* elements (*e.g.* phosphorus (P) and sulfur (S)).

C. elegans have been a successful test bed for pushing the boundaries of microscopy,^{7,8} and are particularly well suited for whole-organism imaging of fundamental biochemistry. Examples span from Raman vibrational spectroscopy for imaging lipid metabolism⁹ to scanning electron microscopy for profiling the *C. elegans* connectome.^{10,11} We have used this nematode to extensively study metal metabolism *via* XFM, conducting population studies,¹² tomography¹³ and X-ray absorption near-edge structure (XANES) spectroscopy¹⁴ to appraise the complex biochemistry of metals *in vivo*. *C. elegans* are highly resistant to ionising radiation,¹⁵ which permits analysis of hydrated and anaesthetised samples for mid-*Z* elements using hard X-rays (> 10 keV).

While hydrated imaging of anaesthetised samples is preferred in principle, the water content increases the absorption of low energy fluorescence, and therefore dehydration aids detection of elements with atomic masses below potassium (K; *Z* < 19). Preserving subcellular distribution of elements is challenging, particularly following chemical fixation. Even brief (< 30 s) formalin fixation of thin tissue sections can cause redistribution and leaching of transition metals and electrolytes.¹⁶ However, we previously demonstrated that cryofixation of *C. elegans* in liquid N₂-cooled propane followed by lyophilisation does not cause significant variation in elemental content or subcellular distribution.¹²

^a Elemental Bio-imaging Facility, University of Technology Sydney, Broadway, New South Wales, 2007, Australia

^b The Florey Institute of Neuroscience and Mental Health, University of Melbourne, Parkville, Victoria, 3010, Australia. E-mail: gmcoll@florey.edu.au; Tel: +61 3 9035 6608

^c Australian Synchrotron, Clayton, Victoria, 3168, Australia

^d ARC Centre of Excellence in Advanced Molecular Imaging, La Trobe Institute for Molecular Sciences, La Trobe University, Melbourne, 3086, Australia

[†] Electronic supplementary information (ESI) available: Experimental methods, figures and movie. See DOI: 10.1039/c5mt00288e

[‡] These authors contributed equally.



Evolving detector capabilities, such as those of the 384-channel Maia reduces sampling overheads by collecting spectra 'on-the-fly' (*i.e.* continuously during a transit across the specimen).¹⁸ The reduced overheads allow scanning of larger samples including whole *C. elegans* in a practical timeframe. Furthermore, this enables spatial oversampling, where data is collected at intervals less than the full width at half maximum (FWHM) of the beam profile. Although the modulation transfer function (MTF) supports the utility of sampling at half of the beam size, in most practical cases this oversampling is not performed due to detector time limitations. Recent upgrades to the Maia detector have improved low-energy sensitivity, thus mitigating this limitation.

Here, we have combined the Maia detector (Rev C), a N₂ environment for reduced Ar fluorescence, sample dehydration and incident energy selections to simultaneously image a broad range of endogenous biological elements from P to strontium (Sr) in wild type *C. elegans*. Specimens were mapped *via* XFM using 12.9 keV and 18.5 keV incident beams. Fluorescence emission was collected by the Maia detector mounted in the backscatter geometry (see ESI† for Experimental Methods). We present highly spatially resolved and correlated images of low-Z elements previously considered as 'difficult' analytes with respect to XFM in biology, whilst also using different modes of imaging to demonstrate the high complementarity possible using a unified imaging approach.¹

Mapping biological samples in a frozen hydrated state can reduce incident beam 'damage', permitting radiation exposure of up to 10¹⁰ Gy, allowing the extended dwell time necessary for the collection of multiple spectra as in XANES analysis¹⁹ or oversampling. However, cryogenic conditions can be prone to artifacts⁴ and retain problematic water content.²⁰ At room temperature, cryofixed and lyophilised *Vicia faba* (fava bean) chromosomes showed no morphological change at radiation doses of up to 10⁷ Gy,²¹ suggesting cryogenic measurements may not always be necessary. Our dehydrated samples received a combined radiation dose of ~10⁶ Gy with no apparent morphological changes in Compton scattering used to identify microstructural features,²² or in known elemental distributions previously described.¹²

Derived Compton maps were used to relate *C. elegans* anatomy to all other measured elements in the hyperspectral image stack (Fig. 1a; full resolution maps available as ESI†). Sulfur was ubiquitously distributed and best recapitulated the majority of anatomical structures (Fig. 1b). Phosphorus also reproduced structural definition of the specimen, though was found at comparatively lower concentrations in the head and full extent of the tail. Consistent with expectations, both elements showed high concentrations within embryos known to be rich in lipids, phospholipids and yolk proteins required for development.

As we have previously shown, Ca and manganese (Mn) were highly compartmentalised along the intestinal lumen,¹³ as was Zn, in addition to being rich within the gonad and embryos, consistent with Zn finger transcription factors necessary for early development. Using the higher incident energy of 18.5 keV, we also found subcellular concentrations of Sr in the most anterior intestine. Strontium commonly substitutes for Ca in biological systems at a greatly reduced concentration,²³ higher

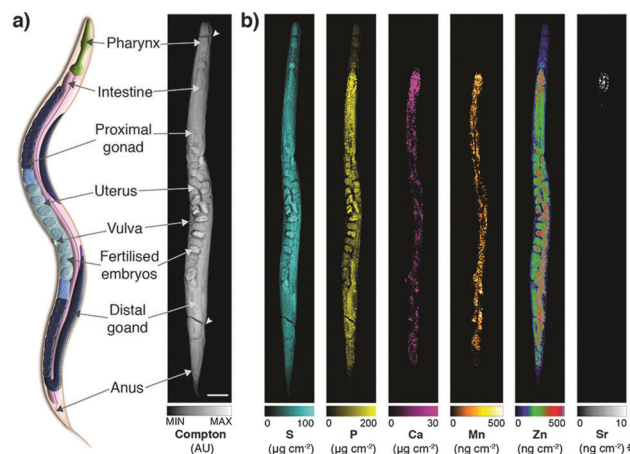


Fig. 1 (a) Schematic representation of major anatomical structures and features of an adult hermaphrodite *C. elegans* (adapted from WormAtlas¹⁷) matched to corresponding features in the XFM map of Compton inelastic scattering. Two fractures in the specimen occurred during cryofixation and lyophilisation (white arrowheads). Scale bar = 50 µm. (b) Corresponding quantitative maps of S, P, Ca, Mn, Zn (all using an incident energy of 12.9 keV) and Sr (18.5 keV; marked with asterisk).

sensitivity of XFM is needed to map to quantify distribution further along the intestinal tract.

Due to minimised time penalties from oversampling, the spatial resolution achieved approached that of light microscopy (approximately 200 nm²⁴), allowing application of statistical approaches to objectively determine if true co-localisation was occurring between specific elements that are both low-Z and highly mobile in the previously hydrated specimen. Potassium and chlorine (presumably as K⁺ and Cl⁻) appeared to have highly correlated cytoplasmic distribution (Fig. 2a). Pearson and Mander's correlation measures of the merged images showed strong association (Pearson's $\rho = 0.708$; Mander's $R = 0.926$). Using Li's method for intensity correlation analysis (ICA),²⁵ which overcomes several limitations of both Pearson and Mander's overlay comparisons, we determined the ICA quotient (*Q*) for the entire organism was 0.234 (+0.5 = perfect correlation; -0.5 = no correlation). Examination of both merged elements and the mapped product of difference from the mean (PDM) used to calculate the overall ICA *Q* showed distinct regions of K-enrichment within the gonad, as well as marked positive correlation in embryos. Interrogation of the pixel (concentration) histograms for each element showed a bimodal distribution indicative of highly enriched K in the gonad. Frequency distribution and PDM *versus* signal intensity (areal concentration) plots further demonstrated a skew towards areas of high K.

Li's ICA *Q* measure is particularly useful for visualising the degree of spatial co-localisation; to demonstrate this we assessed the correlation between Ca and Sr, which within the whole organism was less distinct due to low Sr concentration (ICA *Q* = 0.185). In the anterior intestinal cells where Sr was detectable, we observed high correlation between Ca and Sr in the resulting PDM image (Fig. 2b), consistent with intestinal co-localisation observed in other taxa.²⁶ These results illustrate



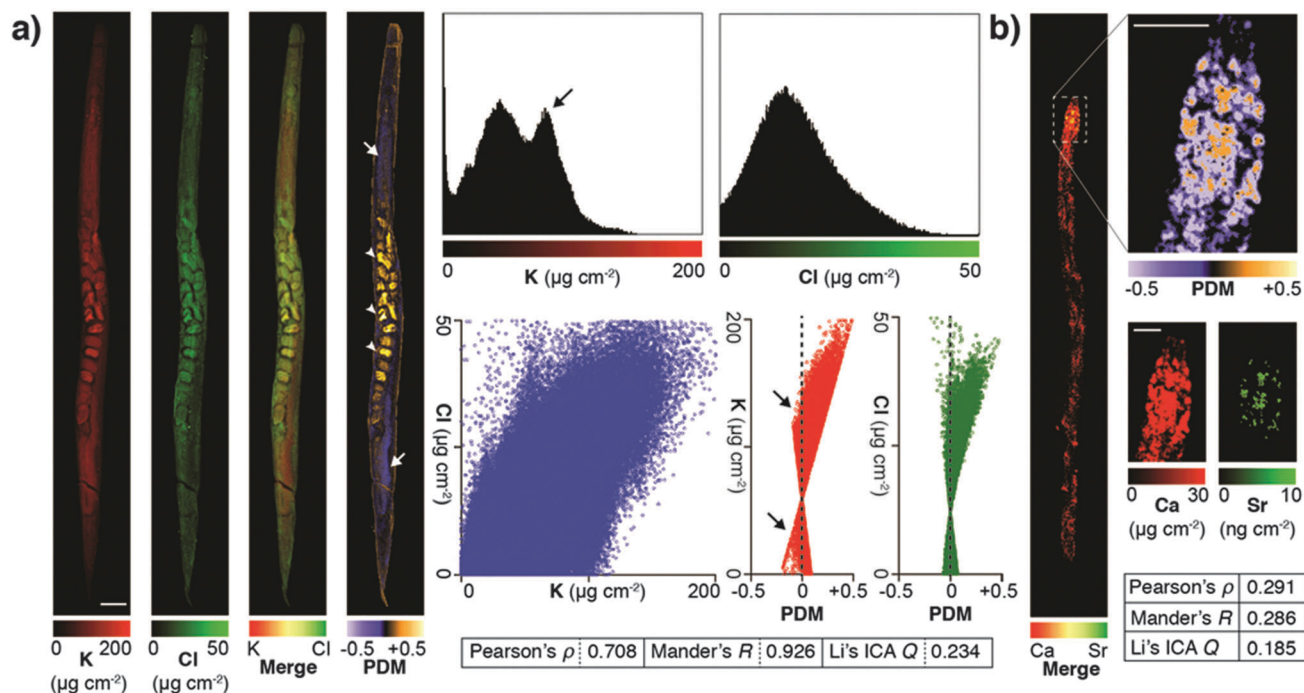


Fig. 2 (a) High abundance and low-Z elements K and Cl were analyzed for co-localisation in an individual *C. elegans* specimen. Images were merged and underwent whole organism correlation analysis using Pearson's, Mander's and Li's intensity correlation analysis (ICA; inset table).²⁵ Visualisation of the product of difference from the mean (PDM; presented on a black background) at high resolution improved interpretation by presenting the ICA quotient (Q) on a pixel-by-pixel basis. Using this method, both elements showed marked correlation in embryos ($0 > Q > +0.5$; white arrowheads), as well as distinct potassium-rich regions within the distal and proximal gonad ($-0.5 < Q < 0$; white arrows). Scale bar = 50 μm . Histograms of pixel values revealed a bimodal distribution for K, consistent with K enrichment in the gonad (black arrow). (b) The advantages of visualising correlation are clear when comparing co-localisation of high abundance Ca with low abundance Sr, which shares similar biochemistry but is close to the XFM limit of detection. Co-localisation is less robust (lower Pearson's ρ , Mander's R and ICA Q) across the whole organism (inset table); though in the anterior intestine where both Ca and Sr are most concentrated shows high spatial correlation ($0 < Q < +0.5$).

that PDM imaging allows both spatial correlation at a sub μm level of detail, as well as the within the whole organism.

The XFM methods used here significantly improved spatial resolution for *in vivo* mapping. Previously we have shown a distribution of iron (Fe) about the intestine at approximately 2 μm resolution.¹² Our sub- μm imaging approach permitted assessment of Fe revealing a level of detail comparable to histological staining and light microscopy. We found that punctate Fe deposits (Fig. 3a) resembled Fe distributions in formalin-fixed, paraffin-embedded sections stained using the Perls method for non-heme Fe (Fig. 3b).²⁷ In addition to localised Fe deposits, XFM mapping also showed a more generalised Fe distribution not seen in Perls staining, indicative of heme. The correspondence between these two diverse imaging modalities suggests that both approaches accurately report on *in vivo* Fe. Although Perls staining is not quantitative, these results differ from those reported by Hackett *et al.*,¹⁶ who suggested formalin fixation alone alters Fe distribution in biological tissue. We suggest that neither radiation damage from XFM, nor extensive chemical processing for histological staining necessarily disturbs the distribution of non-heme Fe in *C. elegans*.

To further explore consistency between complementary imaging methods, we examined the *in vivo* localisation of the dominant Fe storage protein ferritin.²⁸ Using a green fluorescent protein

(GFP) fusion to ferritin we compared high-resolution confocal fluorescence *in vivo* microscopy to XFM mapping and Perls staining (Fig. 3c and d). Distribution of GFP fluorescence, and thereby ferritin localisation, was again remarkably similar to the Fe puncta previously imaged (see Movie, ESI†). Ferritin accounts for almost half of the Fe content of *C. elegans* and therefore represents a good proxy for non-heme Fe. The multiple imaging methods used serve as validation of each respective technique, providing the first consistent representation of subcellular Fe within a whole organism. Future directions of this complementary imaging approach could employ *C. elegans* with mutated genes that affect Fe metabolism, as well as ageing studies (such as those described in James *et al.*¹⁴) to exploit the higher resolution mapping protocol described here. Here we focused on Fe to demonstrate complementary imaging of metal distribution; similar studies could employ the genetically encoded fluorescent calcium sensor GCaMP,²⁹ which has been used in the *C. elegans* model system,³⁰ to compare total body Ca concentration with cell-specific Ca^{2+} content.

In summary, we have demonstrated sub- μm XFM mapping of bio-elements, both rare and ubiquitous, ranging from low-Z to highly abundant transition metals in a model organism ideally suited for studying metal metabolism. Mapping low-Z elements with confidence will facilitate new experimental paradigms.



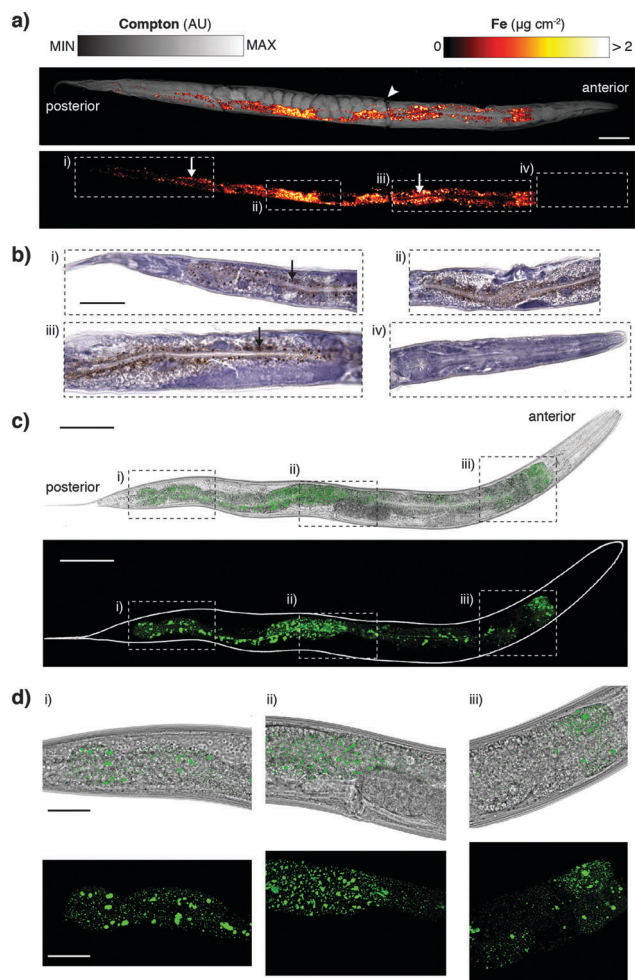


Fig. 3 (a) Iron distribution in a single *C. elegans* sample was overlaid on Compton map showed high concentration along the intestinal lumen, as well as distinct punctate deposits varying from 1 μm in diameter. Scale bars = 50 μm . (b) These features were reflective of non-heme Fe (regions i–iii), confirmed by staining of 5 μm thick sections using 3,3'-diaminobenzidine (DAB)-enhanced Perls staining of an additional specimen. Iron (stained brown) was notably absent in the head (region iv) using both methods. Scale bars = 50 μm . (c) 10 \times brightfield micrograph overlaid with GFP fluorescence and three-dimensional GFP fluorescence-only image of ferritin::GFP distribution in adult *C. elegans*. (d) 40 \times high-resolution confocal micrographs revealed ferritin distribution similar to the punctate deposits of non-heme Fe observed in Perls stained micrographs and XFM mapping. Scale bar = 25 μm .

With image resolution approaching that of light microscopy, implementation of high-level correlative image analysis methods previously reserved for standard fluorescence microscopy are now within reach of contemporary XFM. We also demonstrated how multiple modality imaging provides a greater appreciation of subcellular metal distribution. Using both well-established histochemical analysis and confocal fluorescence imaging provides a more comprehensive picture of Fe distribution within *C. elegans*, an essential element for development and health. A unified approach to imaging using multiple methods accessible to chemists and biologists alike will permit further advances in understanding metal biochemistry.

Acknowledgements

An Australian Research Council Discovery Project (DP130100357) to A. I. B., G. M. and M. D. J. and a UTS Chancellor's Postdoctoral Fellowship to D. J. H. supported this work. We would like to thank the XFM beamline at the Australian Synchrotron, Kirsten Grant, Fransisca Sumardy and Ian Birchall (Florey) for technical assistance, the Caenorhabditis Genetics Center (CGC) supported by the US National Institutes of Health – Office of Research Infrastructure Programs (P40 OD010440) for providing strains, and the Victorian Government's Operational Infrastructure Support Program.

Notes and references

- 1 D. J. Hare, E. J. New, M. D. de Jonge and G. McColl, *Chem. Soc. Rev.*, 2015, **44**, 5941–5958.
- 2 E. Lombi, M. D. Jonge, E. Donner, C. G. Ryan and D. Paterson, *Anal. Bioanal. Chem.*, 2011, **400**, 1637–1644.
- 3 M. J. Pushie, I. J. Pickering, M. Korbas, M. J. Hackett and G. N. George, *Chem. Rev.*, 2014, **114**, 8499–8541.
- 4 J. Deng, D. J. Vine, S. Chen, Y. S. G. Nashed, Q. Jin, N. W. Phillips, T. Peterka, R. Ross, S. Vogt and C. J. Jacobsen, *Proc. Natl. Acad. Sci. U. S. A.*, 2015, **112**, 2314–2319.
- 5 S. Majumdar, J. R. Peralta-Videa, H. Castillo-Michel, J. Hong, C. M. Rico and J. L. Gardea-Torresdey, *Anal. Chim. Acta*, 2012, **755**, 1–16.
- 6 L. Finney, Y. Chishti, T. Khare, C. Giometti, A. Levina, P. A. Lay and S. Vogt, *ACS Chem. Biol.*, 2010, **5**, 577–587.
- 7 B.-C. Chen, W. R. Legant, K. Wang, L. Shao, D. E. Milkie, M. W. Davidson, C. Janetopoulos, X. S. Wu, J. A. Hammer III, Z. Liu, B. P. English, Y. Mimori-Kiyosue, D. P. Romero, A. T. Ritter, J. Lippincott-Schwartz, L. Fritz-Laylin, R. D. Mullins, D. M. Mitchell, J. N. Bembenek, A.-C. Reymann, R. Böhme, S. W. Grill, J. T. Wang, G. Seydoux, U. S. Tulu, D. P. Kiehart and E. Betzig, *Science*, 2014, **346**, 1257998.
- 8 M. Chalfie, Y. Tu, G. Euskirchen, W. W. Ward and D. C. Prasher, *Science*, 1994, **263**, 802–805.
- 9 P. Wang, B. Liu, D. Zhang, M. Y. Belew, H. A. Tissenbaum and J. X. Cheng, *Angew. Chem., Int. Ed.*, 2014, **53**, 11787–11792.
- 10 D. Hall, E. Hartwig and K. Nguyen, in *Caenorhabditis elegans: Cell Biology and Physiology*, ed. J. Rothman and A. Singson, Academic Press, New York, 2012.
- 11 M. Xu, T. A. Jarrell, Y. Wang, S. J. Cook, D. H. Hall and S. W. Emmons, *PLoS One*, 2013, **8**, e54050.
- 12 S. A. James, M. D. de Jonge, D. L. Howard, A. I. Bush, D. Paterson and G. McColl, *Metallomics*, 2013, **5**, 627–635.
- 13 G. McColl, S. A. James, S. Mayo, D. L. Howard, G. F. Moorhead, D. Paterson, M. D. de Jonge and A. I. Bush, *PLoS One*, 2012, **7**, e32685.
- 14 S. A. James, B. R. Roberts, D. J. Hare, M. D. de Jonge, I. E. Birchall, N. L. Jenkins, R. A. Cherny, A. I. Bush and G. McColl, *Chem. Sci.*, 2015, **6**, 2952–2962.
- 15 J. B. Weidhaas, D. M. Eisenmann, J. M. Holub and S. V. Nallur, *Proc. Natl. Acad. Sci. U. S. A.*, 2006, **103**, 9946–9951.



- 16 M. J. Hackett, J. A. McQuillan, F. El-Assaad, J. B. Aitken, A. Levina, D. D. Cohen, R. Siegle, E. A. Carter, G. E. Grau, N. H. Hunt and P. A. Lay, *Analyst*, 2011, **136**, 2941–2952.
- 17 Z. Altun and D. Hall, in *WormAtlas*, <http://www.wormatlas.org/hermaphrodite/hermaphroditehomepage.htm>, 2015.
- 18 C. G. Ryan, D. P. Siddons, G. Moorhead, R. Kirkham, G. De Geronimo, B. E. Etschmann, A. Dragone, P. A. Dunn, A. Kuczewski, P. Davey, M. Jensen, J. M. Ablett, J. Kuczewski, R. Hough and D. Paterson, *J. Phys.: Conf. Ser.*, 2009, **186**, 012013.
- 19 T. Bacquart, G. Devès, A. Carmona, R. Tucoulou, S. Bohic and R. Ortega, *Anal. Chem.*, 2007, **79**, 7353–7359.
- 20 R. Tjallingii, U. Röhl, M. Kölling and T. Bickert, *Geochem., Geophys., Geosyst.*, 2007, **8**, Q02004.
- 21 S. Williams, X. Zhang, C. Jacobsen, J. Kirz, S. Lindaas, J. Hof and S. S. Lamm, *J. Microsc.*, 1993, **170**, 155–165.
- 22 M. D. de Jonge and S. Vogt, *Curr. Opin. Struct. Biol.*, 2010, **20**, 606–614.
- 23 R. Wasserman, *The Transfer of Calcium and Strontium Across Biological Membranes*, Academic Press, New York, 2012.
- 24 S. Goodman, *Medical Cell Biology*, Academic Press, New York, 2007.
- 25 Q. Li, A. Lau, T. J. Morris, L. Guo, C. B. Fordyce and E. F. Stanley, *J. Neurosci.*, 2004, **24**, 4070–4081.
- 26 N. Sugihira, E. Kobayashi and K. T. Suzuki, *Biol. Trace Elem. Res.*, 1990, **25**, 79–88.
- 27 G. Orchard and B. Nation, *Histopathology*, Oxford University Press, Oxford, 2011.
- 28 K. Honarmand Ebrahimi, P.-L. Hagedoorn and W. R. Hagen, *Chem. Rev.*, 2015, **115**, 295–326.
- 29 J. Nakai, M. Ohkura and K. Imoto, *Nat. Biotechnol.*, 2001, **19**, 137–141.
- 30 P. T. McGrath, M. V. Rockman, M. Zimmer, H. Jang, E. Z. Macosko, L. Kruglyak and C. I. Bargmann, *Neuron*, 2009, **61**, 692–699.

